Journal of Renewable Energy and Sustainable Development (RESD) Volume 11, Issue 1, June 2025 - ISSN 2356-8569
http://dx.doi.org/10.21622/RESD.2025.11.1.1236
Received on, 18 February 2025 Accepted on, 27 April 2025 Published on, 12 May 2025

Experimental Study of a Flat Plate Air Solar Collector Fitted with Mini Concentrators

Zakaria Sari Hassoun *1, Mohammed Benramdane 2, Hiba Imane Berrezoug 3, and Khaled Aliane 4

1,4 MECACOMP Laboratory, Department of Mechanical Engineering, Faculty of Technology, University of Tlemcen, Algeria

2 ETAP Laboratory, Department of Mechanical Engineering, faculty of technology, University of Tlemcen, Algeria

3 University Abou-Bekr Belkaïd, Theoretical Physics Laboratory, Tlemcen, Algeria

sarihassounz@yahoo.com, benramdane2006@yahoo.fr, hibaa.imane@yahoo.fr, kh_aliane@yahoo.fr

ABSTRACT

This research presents an experimental examination of the temperature fluctuations occurring in various elements of a flat-plate solar air collector designed for hot air production. To execute this investigation, a novel flat-plate air solar collector incorporating cylindrical mini-concentrators with reflective mirrors (CMCRM) was conceived and constructed. Temperature readings were taken using type K thermocouples strategically positioned on the glazing, the absorber, and within the air space between both. Additional measurements included the ambient air temperature and the collector's outlet air temperature. Data were gathered at diverse times throughout the day on April 13, 2023. The results under ambient temperatures of around 27 °C show that the new solar collector reaches up to 139 °C at the absorber and 129 °C at the air outlet, which is about 30% higher than that of conventional collectors. It maintains high temperatures from 10 a.m. to 4 p.m., making it suitable for continuous-use applications like drying, heating, and industrial processes. Its simple and low-cost design makes it promising for broader deployment, with the potential for further optimization through storage systems or solar tracking.

Index-words: *Solar energy, Airplane solar collector, Cylindrical mini-concentrators with reflecting mirrors, Temperature profile.*

I. INTRODUCTION

The accelerating pace of industrialization, combined with the continuous rise in energy demand, has significantly strained both our finite fossil fuel resources and the quality of the environment. In light of this, there is a growing imperative to explore and develop alternative energy solutions, particularly those based on renewable sources. Among these, solar energy stands out due to its vast potential to meet global energy needs sustainably and with minimal environmental impact. As a result, a wide range of technologies have been developed and continue to evolve to harness this abundant source of energy efficiently [1].

Solar energy has a broad spectrum of uses in thermal processes, like water and air heating, drying, distillation, water pumping, cooking, greenhouse farming, building heating, salt production, and also in photochemical and photobiological conversions, plus hydrogen gas production [2]. Recent reviews, such as the one published in (2025), highlight the growing role of solar thermal collectors in drying systems and underline the need for continuous innovation in collector design and efficiency [3].

A solar flat-plate air collector is a kind of solar thermal apparatus explicitly designed to capture and absorb solar radiation to heat a fluid. The working principle of this collector is relatively straightforward: incoming solar radiation is absorbed by a dark-colored flat surface, the absorber plate, which converts solar energy into heat. This thermal energy is then transferred to the working fluid. Usually, air flows through channels or pipes that touch the absorber plate. Moreover, fluids heated to high temperatures with solar energy can be efficiently utilized for power generation and thermal heating applications [4].

Absorber sheets are often made from metals with great thermal conductivity, like copper, aluminum, or steel, and are generally coated with selective

Volume 11, Issue 1, June 2025 - ISSN 2356-8569
http://dx.doi.org/10.21622/RESD.2025.11.1.1236

substances to maximize the absorption of solar radiation while decreasing thermal losses. The fluid-carrying pipes can either be embedded within or attached to the absorber surface to facilitate efficient heat transfer. The glazing, usually made of glass or transparent plastic, performs a dual function: it allows the transmission of high-frequency solar radiation to the absorber plate while limiting the escape of low-frequency infrared radiation. Moreover, it acts as a physical barrier that restricts convective heat loss by preventing ambient air from circulating over the absorber surface.

Therefore, in order to reduce heat loss, an insulating material, such as fiberglass, is usually placed at the back and sides of the absorber plate, hence providing sealing and thermal insulation. Although plastic materials may be used as glazing, due to their lower cost and higher transmittance, they are less durable compared to glass. Recent experimental comparisons, such as Yidana (2023), have demonstrated that even small modifications, like using nanofluids or optimized coating materials, can significantly enhance heat retention and absorption efficiency in such systems [5]. Likewise, Bouafia and Si Abdallah (2024) also conducted a numerical study in Algeria, showing that collector performance can vary significantly depending on climatic and flow conditions, further highlighting the importance of optimizing design parameters [6]. In this investigation, alterations in tube spacing, length, and diameter were considered to refine the design of the absorber.

II. EXPÉRIMENTAL MATERIALS

For this research, several components were needed, encompassing measurement devices, experimental arrangements, and software tools for data gathering and analysis.

The solar collector utilized in the experimental setup, shown in Figure 1. a, has overall dimensions of 210 cm in length, 112 cm in width, and 13.4 cm in height. The internal test section, where air circulates, measures 200 cm in length, 100 cm in width, and 6.4 cm in height. To assess the impact of forced convection, a fan with a diameter of 12 cm and a rotational speed of 1300 rpm was used, as shown in Figure 1.b.

In addition, mini-concentrators mirrors whose design and functioning are a key component of the system studied. These mini-concentrators feature curved surfaces integrated into the system illustrated in Figure 1.c. The inner face of each concentrator is equipped with a reflective mirror that concentrates the incident solar radiation onto the absorber, thus improving heat gain. The outer face is covered with matte black paint to contribute to the rise of the collector's internal temperature. This configuration is intended to maximize the thermal flux received by the absorber while minimizing losses.

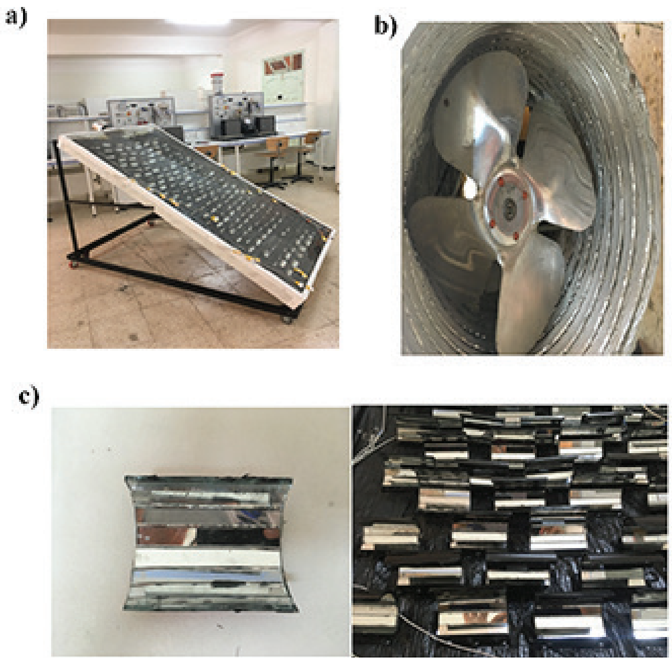

Fig. 1. a) Solar collector under study, b) Fan at the collector output, and c) Mini-concentrators

Temperature measurements were obtained using type K thermocouples made of Nickel-Chrome and Nickel-Aluminum. These thermocouples have a diameter of 0.5 mm and are able to measure temperatures from -50°C to 400°C with an accuracy of ±0.1°C. Type K thermocouples are widely used in experimental research because of their numerous advantages: they display a very linear thermo-electromotive force, demonstrate excellent resistance to oxidation below 1000°C, and provide outstanding thermal stability. Moreover, they can operate across a broad temperature range, from -200°C to 1300°C [7]. Temperature data was acquired using a National Instruments data acquisition system (NI CompactDAQ chassis), as clearly illustrated in Figures 2(a, b) [8].

 Volume 11, Issue 1, June 2025 - ISSN 2356-8569
http://dx.doi.org/10.21622/RESD.2025.11.1.1236

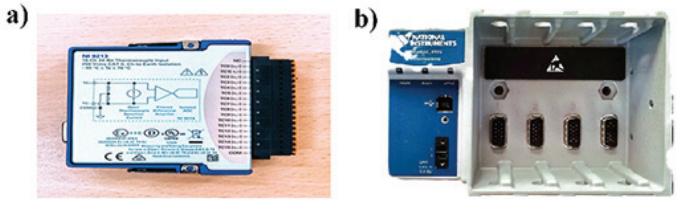

Fig. 2. a) Thermocouple module for temperature measurement, b) Four-pin NI chassis

A CMP6 Pyranometer was used to measure solar irradiance. This instrument is specifically designed to measure global solar radiation on flat surfaces such as flat-plate solar collectors. With a sensitivity of 14.31 μV/W/m², the CMP6 is recognized as a high-quality device suitable for a wide array of experimental applications. Notably, it functions without requiring an external power supply, generating a low-voltage signal (0 to 20 mV) proportional to the intensity of incident solar radiation. However, when a higher output voltage or a 4–20 mA signal is necessary, the use of an AMPBOX is strongly recommended [9]. Finally, To measure airflow velocity at the collector's inlet, an ultrasonic anemometer was employed, offering precise wind speed measurements appropriate for experimental analysis [10].

Data acquisition involves measuring and documenting diverse parameters of the specimens being investigated. A data acquisition system allows the measurement, sampling, and recording of physical values. The gathered data can be processed and examined either in real-time or afterward (Figure 3).

Figure 4 showcases the module's installation inside a chassis, subsequently connected via a USB cable to a computer operating LABVIEW software, facilitating the visualization of temperature fluctuations second by second [11].

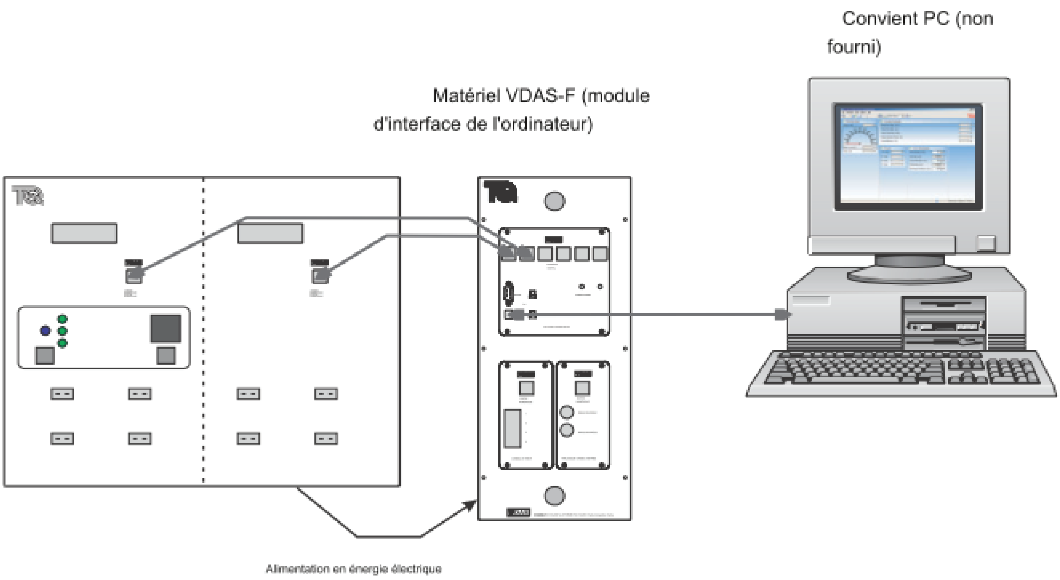

Fig. 3. Test bench provided with software

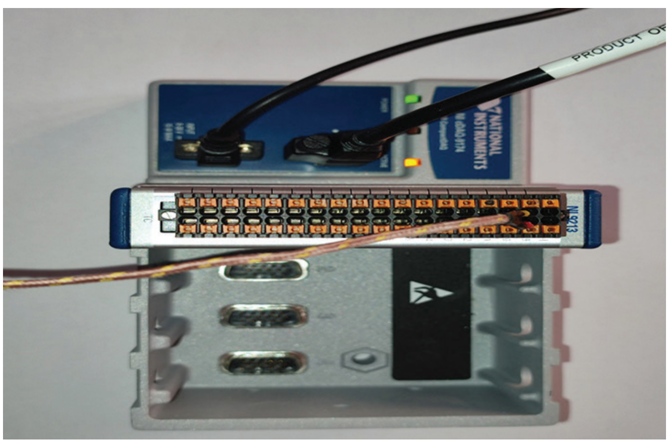

Fig. 4. National Instruments data acquisition system

III. THEORETICAL CALCULATION

Modeling of heat exchanges in an air flat plate solar collector. The method used here assumes that the system operates under steady-state conditions and each element of the insulator has a constant average temperature [12]. The useful power can then be expressed as:

$$P_u = \frac{\dot{m} \text{ x Cp}}{\text{A}} (T_s - T_e) \tag{1}$$

Where:

- Temperature T_e is assumed to be known, while

Volume 11, Issue 1, June 2025 - ISSN 2356-8569
http://dx.doi.org/10.21622/RESD.2025.11.1.1236

T_s needs to be calculated by solving the heat equation (in the fluid domain):

$$\rho Cp \left(\frac{dT}{dt} + \upsilon gradT\right) = d_{iv}(q) + \boldsymbol{\sigma}_T \quad (2)$$

q: The conduction flux

$\boldsymbol{\sigma}_T$: The volumetric heat capacity.

Under steady-state flow conditions and assuming negligible heat conduction within the fluid, the expression above can be rewritten as:

$$\rho Cp\ \upsilon gradT = \boldsymbol{\sigma T} \quad (3)$$

υ: The velocity of the fluid.

Assuming the fluid flows along the x-axis, the equation can thus be expressed as:

$$\rho CpV \frac{dT}{dx} = \boldsymbol{\sigma}_T \quad (4)$$

In addition to the heat flux exchanged through radiation between the absorber and the panel, an additional incident heat flux (Q_g) is also absorbed by the panel. It is very small and is expressed as [13]:

$$Q_g = \boldsymbol{\alpha_g . S_g . G} \quad (5)$$

α_g: The glass absorption coefficient,

S_g: The glass surface area (m^2), and

G: The global radiation.

Equation (6) provides the expression for the heat flux exchanged through convection between the glazing and the surrounding ambient air:

$$\boldsymbol{Q_{cvam} = h_{cvam} . S_v . (T_g - T_{am})} \quad (6)$$

T_{am}: The ambient temperature (K)

h_{cvam}: The convective heat exchange coefficient between glass and ambient air.

The convective heat exchange coefficient may be determined using the Hotel-Woertz correlation given below:

$$h_{cvam} = 5.67 + 3.86\ .V \quad (7)$$

V: The wind speed (m/s).

The heat flux exchanged through radiation between the glazing and sky is given by Equation (7).

Furthermore:

$$Q = h \times S_V \times (T_s - T_g) \quad (8)$$

T_s: The sky temperature (K),

T_g: The glass panel temperature (K),

h (W/m^{2}K): The radiative heat exchange coefficient between the glass and sky.

Heat transfer exchanged by convection between the absorber and the glass panel is given in the following expression:

$$Q = h \times S_{ab} \times (T_g - T_{ab}) \quad (9)$$

T_{ab}: The absorber temperature (K),

S_{ab}: The absorber surface area (m^2),

H_{cabv}: The convective exchange coefficient between the glass panel and absorber (W/m^{2}K).

The convective exchange coefficient is given as:

$$h = Nux \frac{e}{\lambda_{air}} \quad (10)$$

with

$$Nu = 1 + 1.446 \times \left(1 - \frac{1708\ x(\sin(1.8\beta))1.6}{Raxcos(\beta)}\right) x \left(1 - \frac{1708}{Rax\cos(\beta)}\right) + \left(\frac{Rax\cos(\beta)}{5830}\right)^{0.666} - 1 \quad (11)$$

e: The thickness of air space between glass and absorber plate (m),

λ_{air}: The thermal conductivity of air (W/m.K),

β: The inclination angle (rad) of the collector,

Ra: The Rayleigh number.

The heat flux exchanged through radiation between the absorber and the glazing is given by Equation (12):

$$Q = h_{rabv}\ x\ S_{ab}\ (T_v - T_{ab}) \quad (12)$$

It was shown that heat losses in a solar collector mainly result from the temperature difference between the absorber and the surrounding environment. They can be attributed to the three modes of heat transfer, i.e. conduction, convection, and radiation. These losses can be classified into three categories, namely forward losses, backward losses and lateral losses [13].

The forward heat loss coefficient of the solar air collector is given by [14]:

$$U_f = \frac{1}{(\frac{1}{hrvc+hcvam})+(\frac{1}{hcabv+hrabv})} \quad (13)$$

The coefficient of heat loss to the rear of the collector is not very important, as the collector is very well insulated on its back side. It is given as:

$$U_{rear} = \frac{\lambda_{isol}}{e_{isol}} \quad (14)$$

λ_{isol}: The thermal conductivity of insulation (W/K m)

e_{isol}: The insulation thickness (m).

The lateral heat loss coefficient value is lower than that of the rear loss coefficient since the lateral surface of the collector is not very large. It is given by:

$$U_{lat} = \frac{\lambda_{isol}}{e_{isol}} (\frac{S_{lat}}{S_c}) \quad (15)$$

S_{lat}: The collector side surface (m^2)

S_c: The collector surface area (m^2).

Therefore, the overall heat loss coefficient to the outside is the sum of the three coefficients:

$$U_G = U_f + U_{rear} + U_{lat}$$

The instantaneous efficiency of the solar collector is expressed as follows [13]:

η = Useful thermal power per square meter (m^2) of collector / Solar flux incident on collector surface.

The output power = Collected power – Losses

$$\frac{Q_u}{S_c.G} = \frac{S_c[(\alpha\tau).G - U_L(T_{ab} - T_{amb})]}{S_c.G} \quad (16)$$

G: The overall heat loss coefficient to the outside

Q_u: The useful power recovered by the heat transfer fluid (W).

α and τ : The absorber absorption coefficient and the glazing transparency, respectively.

High outlet temperatures in a solar air collector generally indicate that more of the incoming solar energy is being converted into useful thermal energy. This is directly linked to thermal efficiency, which is defined by:

$$\eta = \frac{\dot{m} \times c_p \times (T_{Out} - T_{In})}{A_c \times G} \quad (17)$$

Where:

$\dot{m}$: The mass flow rate of air

C_p: The specific heat of air,

T_{out} and T_{in}: The outlet and inlet air temperatures,

A_c: The collector area,

G: The solar irradiance

IV. RESULTS, DISCUSSION, AND INTERPRETATION

A set of control measures was implemented to ensure consistent and accurate measurements across varying time intervals, especially during peak solar radiation hours. These included Calibrated measurement instruments already seen in section II (e.g., thermocouples and pyranometers), which were used and checked regularly. Data acquisition was automated using the NI Compact DAQ system paired with LabVIEW software, which enabled real-time monitoring and minimized human error. Environmental parameters such as ambient temperature, wind speed, and solar irradiance were continuously logged to account for fluctuations. Steady-state conditions were ensured before each data recording session, allowing for repeatable and stable readings. In case of sudden atmospheric changes (e.g., clouds), those data points were flagged and not considered in the performance analysis. These control measures helped maintain measurement accuracy and reliability throughout the experimental duration.

A. Ambient Temperature and Solar Irradiation

The ambient temperature profile, presented in Figure 5(a), shows a clear variation throughout the day. Between 12:00 p.m. and 4:00 p.m., the ambient temperature steadily increases, ranging from approximately 26 °C to a peak of around 32 °C. This time window corresponds to the period of highest solar irradiance, which naturally contributes to the observed temperature rise. The gradual increase in ambient temperature during these hours plays a significant role in influencing the overall thermal

Volume 11, Issue 1, June 2025 - ISSN 2356-8569
http://dx.doi.org/10.21622/RESD.2025.11.1.1236

performance of the solar collector, as it affects both the heat losses to the surroundings and the efficiency of heat transfer within the system.

The solar irradiation trend is illustrated in Figure 5(b). Prior to 10:00 a.m., solar irradiance remains relatively low, not exceeding 200 W/m². This can be attributed to the low solar elevation angle and the presence of morning atmospheric attenuation. However, after 10:00 a.m., a significant rise in solar irradiation is observed, with values rapidly increasing to reach a peak of approximately 1000 W/m². This sharp increase indicates the onset of strong and direct sunlight as the sun ascends in the sky, providing optimal conditions for solar energy collection during the midday period.

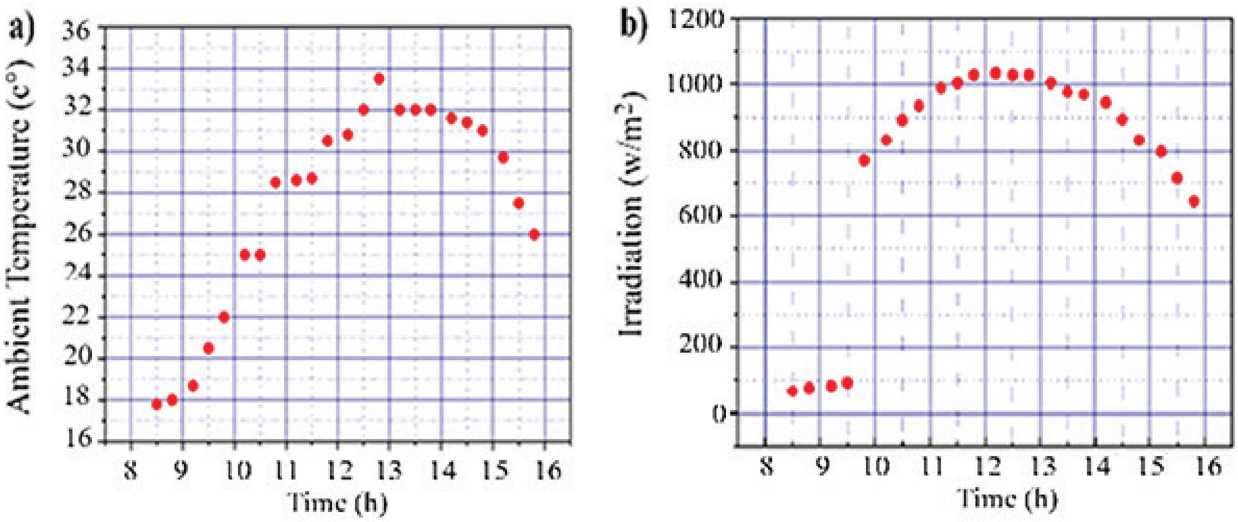

Fig. 5. a) Ambient temperature and b) Solar irradiation

B. *Glazing Temperature and Absorber Temperature*

Figure 6 (a) presents the variation in temperature measured at the glazing surface of the solar collector. At around 12:00 p.m., the glazing temperature reaches its peak, exceeding 70 °C, which corresponds to the period of maximum solar irradiation. Following this peak, a gradual decline in temperature is observed, with the glazing temperature decreasing steadily to approximately 55 °C by 4:00 p.m. This downward trend is likely due to the reduction in solar intensity during the afternoon hours, combined with increased heat losses through radiation and convection as ambient conditions begin to cool. These results align with those reported in Jamil et al., 2022 [], where glazing temperature rises up to ~20 °C above ambient, and glazing losses can account for 36.67 % in summer and 51.40 % in winter of the total solar input energy.

The temperature distribution of the absorber is illustrated in Figure 6 (b). It is observed that the absorber temperature reaches a maximum of approximately 139 °C at around 12:30 p.m., coinciding with the period of highest solar irradiance. After this peak, the temperature begins to decline progressively, reaching about 95 °C by 4:00 p.m. This temperature drop follows the natural reduction in solar intensity during the afternoon hours. The notably high temperatures recorded in this experimental setup highlight the enhanced thermal performance of the modified solar collector. Compared to a conventional flat plate air solar collector, the temperatures achieved here are significantly higher, indicating improved solar energy capture and heat retention, likely due to the use of mini-concentrator mirrors and optimized design features. Comparées à un capteur solaire à air plan classique, les températures atteintes ici sont significativement plus élevées, indiquant une meilleure capture de l'énergie solaire et une meilleure rétention de la chaleur, probablement grâce à l'utilisation de mini-miroirs concentrateurs et à des caractéristiques de conception optimisées. Une tendance similaire a été observée dans Asif et al., 2022 [16], qui ont démontré que la température de l'absorbeur est très sensible à l'épaisseur de la couche d'air et à la configuration du vitrage, affectant la capacité de rétention de chaleur et le comportement des pertes convectives.

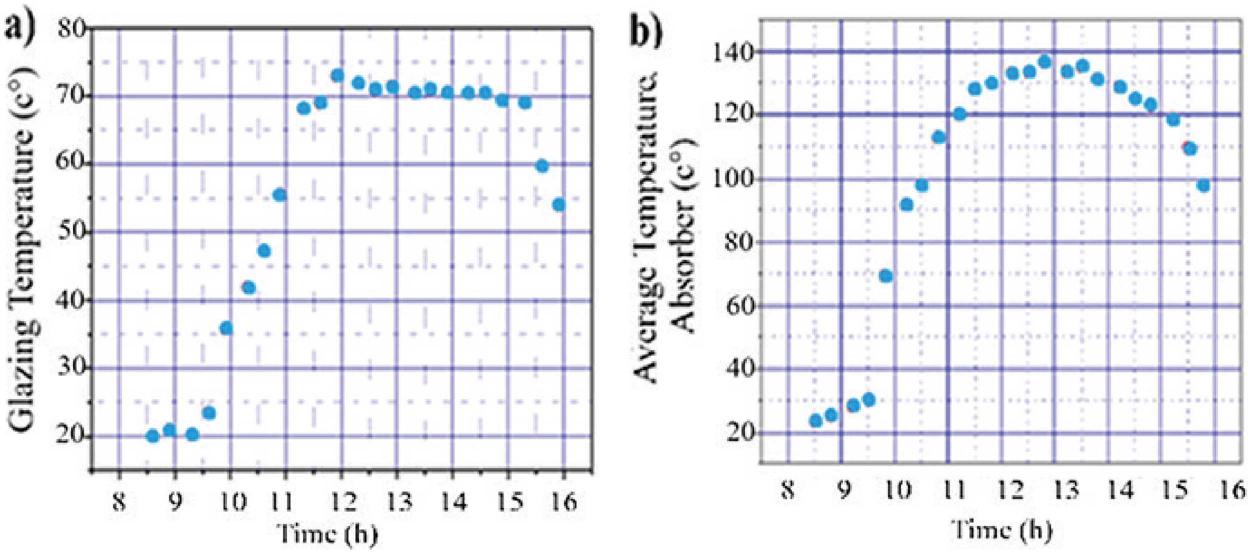

Fig. 6. a) Glazing temperature and b) Absorber temperature

C. The Air Temperature inside the Collector and at the Collector Outlet

The air temperature distribution inside the solar collector is shown in Figure 7 (a). As observed, the outlet air temperature rises steadily throughout the morning, reaching a peak of approximately 129 °C at around 1:00 p.m. This maximum corresponds to the period of optimal solar irradiation and thermal energy accumulation within the collector. Following this peak, the outlet air temperature gradually decreases, reaching approximately 96 °C by 4:00 p.m., in line with the natural decline in solar intensity during the late afternoon. These results confirm the efficient heat transfer between the absorber and the circulating air and underscore the collector's ability to deliver high-temperature air, which is particularly beneficial for thermal applications such as drying or space heating,

Typically, standard flat plate air collectors reach outlet temperatures between 90 °C and 100 °C under similar solar irradiance conditions (800–1000 W/m²), as reported by Belessiotis & Delyannis [17], Kalogirou [18], and Duffie & Beckman [19]. This performance range has been corroborated by recent studies, such as the one by Jebaraj and Khan [20], which reviewed various solar drying systems and highlighted that conventional flat plate collectors typically achieve outlet temperatures within this range under comparable conditions. In contrast, the proposed design achieved an absorber temperature of 139 °C and an outlet air temperature of 129 °C, resulting in a performance improvement of nearly 30%, which highlights the effectiveness of the integrated mini-concentrators in enhancing thermal efficiency. At the same time, this particular study focused primarily on the experimental temperature characterization; the thermal efficiency can be estimated using the standard expression shown in section III (eq.17).

Figure 7 (b) illustrates the air temperature distribution at the outlet of the solar collector. The data reveals that the outlet air temperature reaches a peak value of approximately 115 °C at around 1:00 p.m., reflecting the period of highest solar gain. Subsequently, the temperature gradually decreases over the afternoon, reaching about 90 °C by 4:00 p.m. This decline is consistent with the reduction in solar irradiation and ambient temperature. The elevated temperatures achieved during the midday period indicate effective thermal energy conversion and highlight the system's suitability for applications requiring medium to high-temperature air output. Similar trends were observed in the study by Hamdan et al. [1], where a solar air heater incorporating evacuated tubes and nano-enhanced phase change materials (NE-PCM) reached an outlet temperature of 116 °C at 1:00 p.m. with an airflow rate of 0.006 kg/s, which then declined to around 90 °C by 4:00 p.m. under comparable irradiance conditions. This comparison underscores the high thermal performance of the proposed system, which, even without thermal storage materials like NE-PCM, achieves similarly elevated temperatures, thereby affirming its efficiency and applicability in processes such as drying, pre-heating, and space heating.

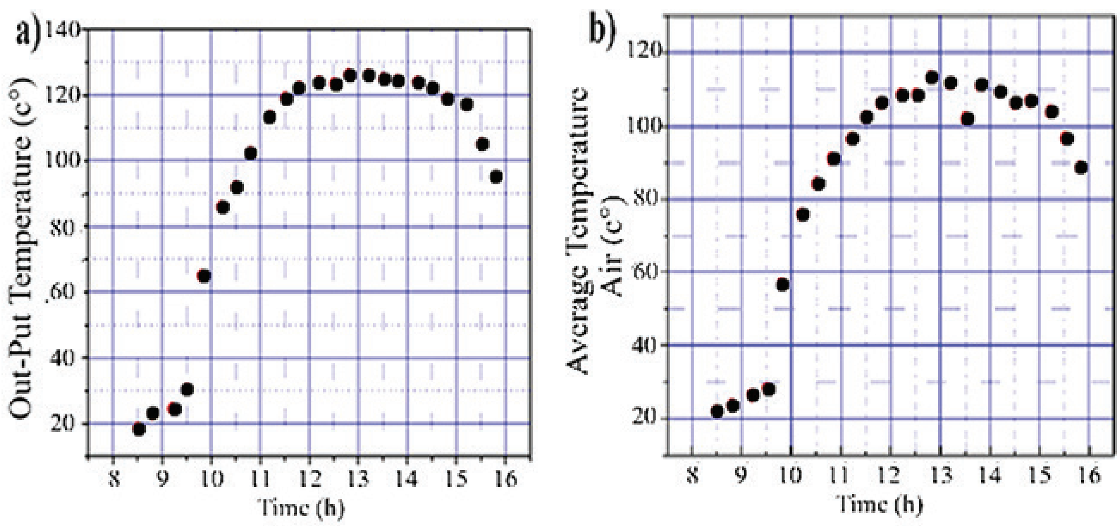

Fig. 7. Air temperature: a) inside the collector and b) at the collector outlet

V. CONCLUSION

This study provided an in-depth characterization and analysis of the thermal performance of a modified air solar collector, incorporating mini-concentrator mirrors and optimized design features. The measurement and control protocols implemented ensured reliable and reproducible results, allowing for a precise interpretation of the thermal phenomena observed.

The analysis of environmental parameters such as ambient temperature and solar irradiation highlighted the significant impact of external conditions on the collector's performance. The ambient temperature exhibited a regular variation, directly influencing the system's thermal performance, while the solar irradiation reached optimal values after 10:00 a.m., promoting efficient energy collection during peak solar hours.

The glazing and absorber temperatures reached notably high values, with the glazing temperature exceeding 70°C and the absorber temperature reaching 139°C. These values indicate the enhanced performance of the modified solar collector compared to conventional flat plate collectors. This approximately 30% improvement in thermal performance can be attributed to the integration of mini-concentrator mirrors and the optimized collector design. These results align with previous studies, such as Asif et al. (2022), which also demonstrated the significant role of air gap thickness and glazing configuration in heat retention.

Regarding the air temperature inside the collector and at the collector outlet, the results showed outlet temperatures reaching up to 129°C, higher than those observed for conventional flat plate air collectors, which typically range from 90°C to 100°C under similar solar irradiation conditions. This enhanced performance highlights the efficient thermal energy transfer between the absorber and circulating air, underscoring the system's ability to deliver high-temperature air, which is ideal for thermal applications such as drying or space heating.

Finally, the experimental results obtained confirm the high efficiency of the modified air solar collector, which demonstrates elevated thermal performance and suitability for applications requiring medium to high-temperature air output. These findings pave the way for continued advancements in solar thermal energy collection, particularly through the integration of advanced technologies such as mini-concentrator mirrors and optimized system configurations.

References

[1] S. Suman, Mohd. K. Khan, and M. Pathak, "Performance enhancement of solar collectors—A review," *Renewable and Sustainable Energy Reviews*, vol. 49, pp. 192–210, Sep. 2015, doi: 10.1016/j.rser.2015.04.087.

[2] K. M. Pandey and R. Chaurasiya, "A review on analysis and development of solar flat plate collector," 2017. doi: 10.1016/j.rser.2016.09.078.

[3] J. S. and M. Y. Khan, “A review on solar dryers to evaluate the performance and drying characteristics for agricultural products,” *Renewable Energy and Sustainable Development*, vol. 11, no. 1, p. 22, Jan. 2025, doi: 10.21622/resd.2025.11.1.1039.

[4] A. Robles, V. Duong, A. J. Martin, J. L. Guadarrama, and G. Diaz, “Aluminum minichannel solar water heater performance under year-round weather conditions,” *Solar Energy*, vol. 110, pp. 356–364, Dec. 2014, doi: 10.1016/j.solener.2014.09.031.

[5] A.-M. Y. Yidana, “2d solar thermal direct absorption comparison between gold and silver nanoparticle,” *Renewable Energy and Sustainable Development*, vol. 9, no. 2, 2023, doi: 10.21622/resd.2023.09.2.032.

[6] S. Bouafia and M. Si Abdallah, “Numerical study of a solar PV/thermal collector under several conditions in Algeria,” *Renewable Energy and Sustainable Development*, vol. 10, no. 2, p. 233, Sep. 2024, doi: 10.21622/resd.2024.10.2.900.

[7] M. H. Nguyen, S.-E. Ouldboukhitine, S. Durif, V. Saulnier, and A. Bouchair, “Passive fire protection of steel profiles using wood,” *Eng Struct*, vol. 275, p. 115274, Jan. 2023, doi: 10.1016/j.engstruct.2022.115274.

[8] T. Baycheva-Merger, M. Sotirov, S. Holmgren, and A. Selter, “Institutional and Actor-Oriented Factors Constraining Expert-Based Forest Information Exchange in Europe: A Policy Analysis from an Actor-Centred Institutionalist Approach,” *Forests*, vol. 9, no. 3, p. 129, Mar. 2018, doi: 10.3390/f9030129.

[9] A. Manzano, M. L. Martín, F. Valero, and C. Armenta, “A single method to estimate the daily global solar radiation from monthly data,” *Atmos Res*, vol. 166, pp. 70–82, Dec. 2015, doi: 10.1016/j.atmosres.2015.06.017.

[10] H. Alexandersson, “A homogeneity test applied to precipitation data,” *Journal of Climatology*, vol. 6, no. 6, pp. 661–675, Jan. 1986, doi: 10.1002/joc.3370060607.

[11] M. Bitter *et al.*, “Doppler-Broadening Measurements of X-Ray Lines for Determination of the Ion Temperature in Tokamak Plasmas,” *Phys Rev Lett*, vol. 42, no. 5, pp. 304–307, Jan. 1979, doi: 10.1103/PhysRevLett.42.304.

[12] L. A. Tagliafico, F. Scarpa, and M. De Rosa, “Dynamic thermal models and CFD analysis for flat-plate thermal solar collectors - A review,” 2014. doi: 10.1016/j.rser.2013.10.023.

[13] Mr S. BEKKOUCHE, “Modeling the Thermal Behavior of Some Solar Devices. ‘Electronics and Modeling’ option,” Doctoral thesis, Abou-bakr-Belkaid University , Tlemcen, 2008.

[14] P. Wibulswas, “Solar Thermal Processes in Thailand: A Study on Forced Convection Hut Drying,” *National Energy Administration, Ministry of Science, Technology and Energy, Thailand*.

[15] M. Jamil et al., “Étude sur les pertes thermiques par vitrage dans les capteurs solaires à air,” *Revue des Énergies Renouvelables*, vol. 25, no. 4, pp. 123–135, 2022.

[16] M. Asif et al., “Impact de l’épaisseur de la couche d’air et de la configuration du vitrage sur la température de l’absorbeur d’un capteur solaire à air,” *J Sol Energy Eng*, vol. 144, no. 2, p. 021003, 2022.

[17] V. Belessiotis and E. Delyannis, “Solar drying,” *Solar Energy*, vol. 85, no. 8, pp. 1665–1691, Aug. 2011, doi: 10.1016/j.solener.2009.10.001.

[18] S. A. Kalogirou, “Solar thermal collectors and applications,” *Prog Energy Combust Sci*, vol. 30, no. 3, pp. 231–295, 2004, doi: 10.1016/j.pecs.2004.02.001.

[19] J. A. Duffie and W. A. Beckman, *Solar Engineering of Thermal Processes* , 4th Edition. Wiley.

[20] J. S. and M. Y. Khan, “A review on solar dryers to evaluate the performance and drying characteristics for agricultural products,” *Renewable Energy and Sustainable Development*, vol. 11, no. 1, p. 22, Jan. 2025, doi: 10.21622/resd.2025.11.1.1039.